Inorganic Chemistry Research

Article

Green Synthesis of Carbon Quantum Dots from *Trigonella Foenum-graecum L.* Seeds Extract and Investigation of their Cytotoxicity and Photocatalytic Properties

Marzieh Rezaei[a], Azadeh Hekmat[a], Jamshidkhan Chamani[b], Kayvan Sadri[c], Majid Darroudi[c,d,*]

[a]*Department of Biology, Faculty of Science, Science and Research Branch, Islamic Azad University, Tehran, Iran*
[b]*Department of Biology, Faculty of Sciences, Mashhad Branch, Islamic Azad University, Mashhad, Iran*
[c]*Nuclear Medicine Research Center, Mashhad University of Medical Sciences, Mashhad, Iran*
[d]*Department of Basic Medical Sciences, Neyshabur University of Medical Sciences, Neyshabur, Iran*

Received: June 25, 2022; Accepted: October 20, 2022
Cite This: *Inorg. Chem. Res.* **2022**, *6*, 107-113. DOI: 10.22036/icr.2022.348862.1132

Abstract: In this work, carbon quantum dots (CQDs) were synthesized through a simple and efficient hydrothermal method with the usage of *Trigonella foenum-graecum L.* seeds as a low-cost and green material. The synthesized CQDs was confirmed through the results of FTIR, FESEM, EDAX, TEM, UV-Vis, and PL analyzes. The photocatalytic activity of CQDs was investigated for the degradation of Rhodamine B (RhB) dye as a target pollutant, resulting in the photodegradation percentage of 92% during 80 min, which indicates the effective role of CQDs in RhB decolorization under UVA-light irradiation. Also, the biocompatibility of CQDs was evaluated on the cancer CT26 cell line through the MTT assay and the concentration-dependent cytotoxicity of CQDs was confirmed along with the IC_{50} value of about 826 µg/mL.

Keywords: Carbon quantum dots, Hydrothermal method, *Trigonella foenum-graecum L*, Cytotoxicity, Photocatalytic

1. INTRODUCTION

The carbon nanomaterials, such as fullerene, nan diamonds, carbon nanotubes, and CQDs, attracted the attention of many researchers due to their high potential for environmental and technical applications.[1] The strong and adjustable fluorescence emission of quantum dots has led to their extensive usage for many years, however, the high toxicity that accompanied the application of heavy metals created certain limitations in the production of semiconductor quantum dots.[2] Therefore, the suitability of CQDs as a replacement for these materials was confirmed due to their low toxicity, availability, water-solubility, ineffective chemical, and low costs.[3] As it is known, CQDs are nanoparticles with a size range of <20 nm [4] that were accidentally discovered by Xu. *et al* in the process of purifying single-walled carbon nanotubes from the crude soot in 2004;[5] the label of "CQD" was chosen by Sun. *et al* in 2006.[6,7] Next to their amorphous or crystalline morphology with SP^2 carbon clusters, CQDs contain a variety of surface functional groups such as –OH and –COOH.[8] So far, various synthesizing methods were reported for this product such as glycerol pyrolysis, microwave method, solvothermal, hydrothermal, ultrasonic method, electrochemical oxidation method, and thermal carbonization.[9-15] Nevertheless, hydrothermal proved to be a superior technique due to offering a facile, low temperature, effective, single-step, and greener route.[16] The CQDs have a wide range of applications throughout the fields of bioimaging, drug delivery, photocatalysis, electrocatalysis, biosensors, photodynamic therapy, and chemical sensing.[17-23] Meanwhile, the initiation of photocatalytic researches and studies on CQDs has triggered 6 years ago, and accordingly, its unique functionality as photocatalysts were discovered as a result of its ability to cover a wider range of light than semiconductor photocatalysts. The dyes decolorization is commonly exerted to evaluate the photocatalytic applications of CQDs. As persistent pollutants, organic dyes became an important issue in biological pollution due to being exerted in many applications including leather, paper, textile industries, etc.[24-26] This widespread usage arose the obstacle of organic dyes degradation and consequently, the attention of many researchers was attracted towards the synthesis of effective photocatalysts for performing successful degradation processes.[27] In this work, CQDs were prepared through a facile, green, and

effective method with the usage of *Trigonella foenum-graecum L.* (TFL) seeds extract. The obtained product was used for the degradation of various organic dyes from water solutions, while optimizing the applied conditions such as the type of dye and pH in the presence of CQD as the photocatalyst. Also, the biocompatibility of CQDs was evaluated on cancer CT26 cell line through the MTT assay.

2. EXPERIMENTAL

Materials and measurements

The fresh TFL seeds were collected from the northern mountain foothills of Khorasan Razavi province, Iran. The Methylene blue (MB), Rhodamine B (RhB), Methyl orange (MO), and Eriochrome Black T (EBT) dyes were purchased from Sigma-Aldrich Co. All of the materials were ascertained to be of analytical grade and used without any purification.

Preparation of CQDs

The synthesis of CQDs was achieved through a facile and one-step hydrothermal method. Initially, 1.0 g of TFL seeds were washed with distilled water and left aside to dry the excess water to be ground afterward. Then, the obtained powder was added to 100 mL of water to be stirred at 60 °C for 2 h. The mixture was transferred into a Teflon-lined stainless steel autoclave and heated at 180 °C for 4 h. The autoclave was allowed to be naturally cooled down to room temperature. The produced dark brown solution was centrifuged at 12,000 rpm for 15 min and filtered by a 0.22 µm filter membrane to separate the black insoluble carbonaceous particles. As the last step, the obtained solution was freeze-dried and stored at 4 °C. The synthesis schematic of CQDs is exhibited in Fig. 1.

Fig. 1. The synthesis schematic of CQD from *Trigonella foenum-graecum L* seeds extract.

Characterization of CQDs

The infrared spectrophotometer (AVATAR 370) was exerted to record the FTIR spectrum, while the XRD pattern was obtained by the usage of an instrument (X'PertPro−MPD) with Cu K_α radiation. In addition, the UV-Vis absorption spectrum was recognized through a UV-Vis spectrophotometry (CE9500) and the PL spectra were determined by utilizing a fluorescence spectrophotometer (FL4600). The FESEM images were achieved by the means of scanning electron microscopy (JCM) and the EDX analyses were performed using the FESEM instrument, which was equipped with an energy dispersion spectrometer of X−ray with a voltage acceleration of 20 kV. We also exerted a transmission electron microscope (AB LEO912) to attain the TEM images, while using a zeta compact analyzer to conduct the DLS and Zeta potential measurements.

Evaluation of cytotoxicity effect

In this work, the application of MTT (5,4-dimethylthiazole-2-yl) -5,2-diphenyltetrazolium bromide) assay was considered to evaluate the cytotoxic effects of CQDs by measuring the survival rate of cancer CT26 cell line. For this purpose, once the surface of cells was washed with PBS, trypsin was added to deform the cells from their elongated state towards the spherical state. Then, 2×10^4 cells were counted and placed in 96-well plates, containing 200 µL of complete culture medium, for 24 h to adhere the cells to the bottom of the plates and maintain their stability. In the following, the cells were treated with different concentrations of CQDs to be placed in an incubator at 37 °C in a CO_2 atmosphere for 48 h. Once the supernatant culture medium was drained, we appended 20 µL of MTT solution (5 µg/mL) to each well and had them placed in an incubator at 37 °C for 4 h. As the next step, DMSO (40 µL) was added to every well for dissolving the produced formazan crystals. The absorbance of each well was measured at 570 nm by an Elisa reader. We also determined the survival rate of cells by comparing the cells absorption ratio of the treatment group with the control group (zero concentration), while the inhibitory concentration (IC_{50}) was considered to be the concentration at which 50 % of the cells were destroyed.

Photocatalytic activity

We investigated the photocatalytic activity of synthesized CQDs throughout the degradation of MO, MB, RhB, and EBT dyes. Initially, 3.0 mg of CQDs was added to 100 mL of dye solution (10^{-5} M) and stirred in dark for 30 min to achieve an equilibrium in the adsorption and desorption. Then, the solution was placed under a UVA-light source (20 W) at a distance of 20 cm from the reaction vessel top while being stirred. Meanwhile, 2 mL of the solution was collected in regular intervals and its absorption spectrum was determined through UV-Vis spectrophotometry. The degradation percentage of dye was calculated by the application of Eq. 1 [28].

$$Degradation\ (\%) = \frac{A_0 - A_t}{A_0} \quad (1)$$

A_0 = Intial absorption of the solution
A_t = Final absorption of the solution

3. RESULTS AND DISCUSSION

FTIR

The conduction of FTIR analysis provided data on the functional groups that exist throughout the surface of CQDs (Fig. 2). Accordingly, the observed broad band at 3411 cm^{-1} was related to the O–H and N–H stretching vibrations of –OH, –COOH, and –NH groups. Additionally, the absorption peak of C–H stretching vibration was observed at 2927 cm^{-1},[29] while the detected band at 1760 cm^{-1} was assigned to the stretching vibration of the C=O.[30] The absorption bands at 1643 and 1406 cm^{-1} were related to the stretching vibrations of C=O and C–N groups[31]. Lastly, the stretching vibration of the C–O band was recorded at 1074 cm^{-1}.[32]

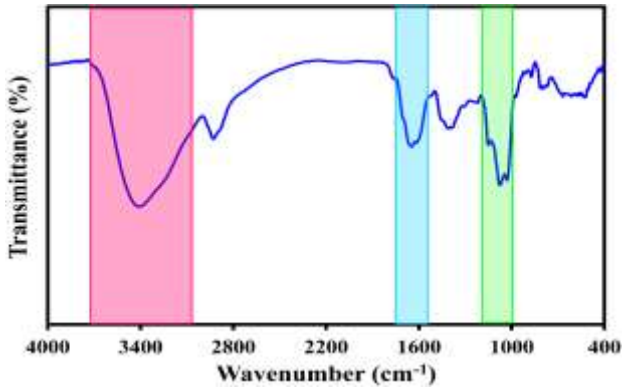

Fig. 2. FTIR spectrum of the CQDs.

XRD pattern

The XRD pattern of CQDs was recorded on a diffractometer equipped with graphite monochromatized Cu K_α (λ = 1.54 A°) radiation throughout the 2θ range of 10° to 70°. Once the XRD sample was pressed on the glass substrate, a weak peak appeared at 51° that was in correspondence to the graphite (100) crystal plane, which is exhibited in Fig. 3. Furthermore, a narrow diffraction peak was observed at 20° that was related to the (002) plane and could be considered as a sign of CQDs crystallinity structures.[33]

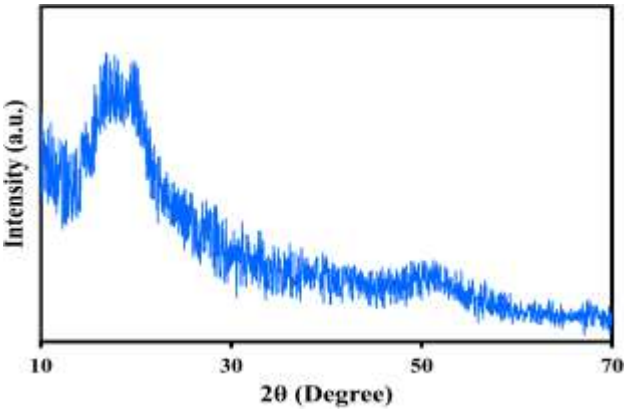

Fig. 3. The XRD pattern of the CQDs.

FESEM-EDX

The morphology of CQDs was studied by the usage of FESEM images and the obtained results displayed the particle's spherical structure along with their outmost satisfying dispersion (Fig. 4a). The EDX analysis was performed on the element composition of synthesized CQDs. According to the provided data in Fig. 4b, this product is mainly composed of carbon (C), oxygen (O), and nitrogen (N) elements with weight percentages of 49.52, 42.89, and 7.59%, respectively.

TEM image

TEM analysis was performed to identify the morphology and size of synthesized CQDs, which resulted in

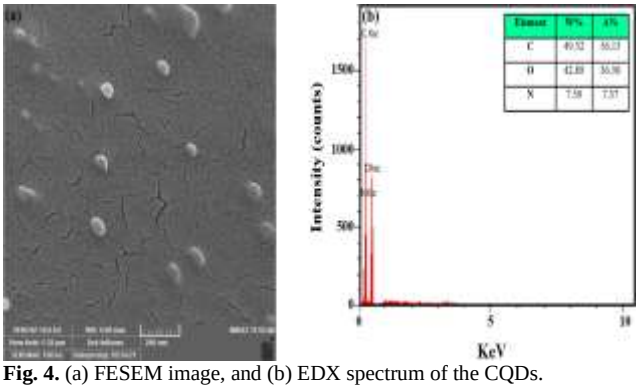

Fig. 4. (a) FESEM image, and (b) EDX spectrum of the CQDs.

exhibiting their quasi-spherical structure and satisfying dispersion (Fig. 5a)[34]. The average size of CQDs can be estimated through the random counting of their sizes, which ranged from 2 to 12 nm while their average size was displayed in the histogram to be 6.98 nm (Fig. 5b).

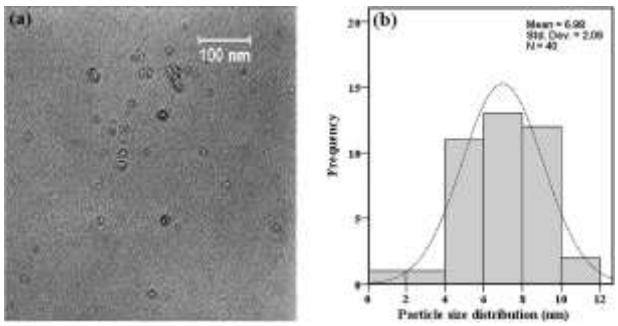

Fig. 5. (a) TEM image, and (b) particle size histogram of the synthesized CQDs.

Zeta potential

The DLS analysis was performed to determine the size of CQDs in an aqueous medium. In conformity to Fig. 6a, the average size of hydrodynamic diameter was 224 nm, which is much larger than the reported size of TEM images. This difference can be attributed to the hydrated layer from the surface of CQDs.[35] As it is known, the zeta potential of a dispersed system represents the scale of electrostatic degree in between its adjacent charged particles, and in this regard, measuring this factor can provide valuable data for examining the adhesion of particles[36]. Considering how the zeta potential of CQDs was calculated to be -4.0 mV at pH equal to 6, the achieved negative value indicates the existence of a repulsive force between the particles (Fig. 6b).[37] Therefore, the aqueous solution of CQDs in a dispersed system was proved to be more stable than a pure system, while there was a lack of observing any agglomeration even after being stored for 6 months.

Optical properties of CQDs

The remarkable optical properties of CQDs are one of the significant and accountable factors for their

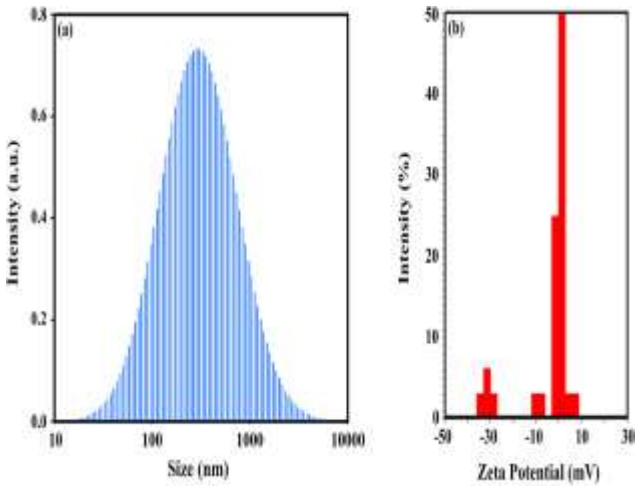

Fig. 6. (a) DLS analysis, and (b) Zeta potential of the CQDs.

effective application. The UV-Vis spectrum of CQDs at a wavelength range of 260 to 800 nm is demonstrated in Fig. 7a. The adsorption peak at 280 nm was related to n→π* transitions from the C=O band.[38] According to the provided inside photo in Fig. 7a, the emitting of green light as the aqueous solution of CQDs is exposed to UVA-light (365 nm) is caused by the fluorescence of CQDs. In addition, the bandgap energy of CQDs was calculated by the exertion of the Tauc equation (Eq. 2), in which $h\nu$ refers to the photon energy, E_g represents the gap band energy, and n is equal 0.50 for directly allowed transmissions. From the extrusion of the linear part of the plot curve $(\alpha h\nu)^2$ vs. hν (Fig. 7b), the value of band gap was calculated to be 3.9 eV. Considering how the band gap energy is greater than ($E_g \geq 3$), it is concluded that the CQDs can be excited only under UVA-light and their functionality is dependent on optical activity.[39]

$$\alpha h\nu = A\left(h\nu - E_g\right)^n \quad (2)$$

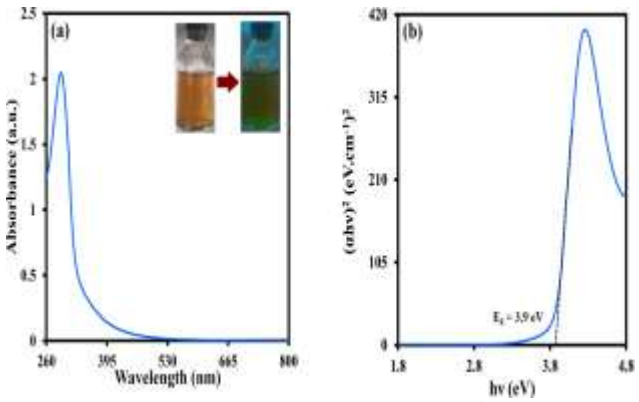

Fig. 7. (a) UV-Vis spectrum, and (b) bandgap energy of the CQDs.

The excitation-dependent emission spectra of CQDs at the excitation wavelength range of 360 to 460 nm are exhibited in Fig. 8. The maximum emission was achieved at the excitation wavelength of 380 nm with an emission wavelength of 460 nm. The fluorescence seemed to be intensified as the excitation was increased from 360 to 410 nm while facing a reduction as a result of increasing the excitation from 410 to 460 nm. This outcome may be due to the size of CQDs, as well as their aromatic conjugate structure and available sp^2 sites.[40]

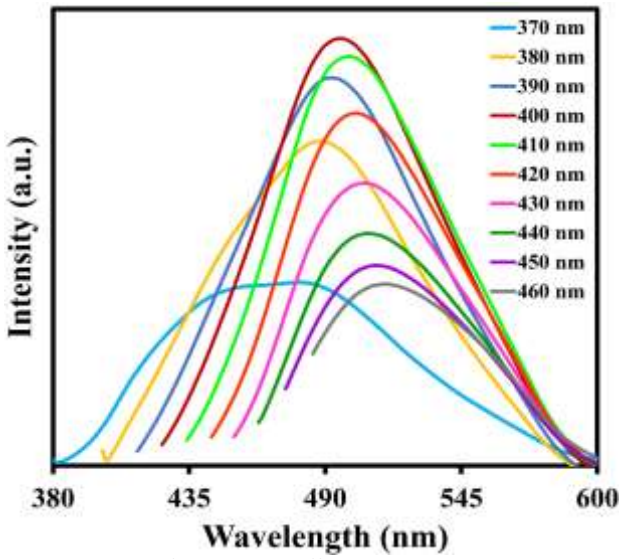

Fig. 8. PL spectra of the CQDs at different excitation wavelengths.

Evaluation of photocatalytic activity

To evaluate the photocatalytic activity of synthesized CQDs throughout the degradation of organic dyes, we selected four different dyes including MB, MO, EBT, and RhB. According to the outcomes, the formation of reactive oxygen species (ROS) in the aqueous medium resulted in achieving a high degradation percentage for all of the experimental dyes in the presence of CQDs under ultraviolet light at 80 min. As it is displayed in Fig. 9a, the degradation percentages of MO, MB, EBT, and RhB dyes were reported to be 24, 26, 30, and 71%, respectively. Therefore, RhB dye with the highest percentage of degradation was selected as the optimal dye to be studied for gathering further data on the photocatalytic activities of this product. The effect of pH on the photocatalytic degradation of RhB was investigated under UVA-light. According to the exhibited results in Fig. 9b, the RhB degradation was investigated at the pH of 4, 7, and 9, which was observed to be increased as the value of pH was intensified. This observation can be attributed to the existing amounts of OH^- and H^+ in the reaction medium, since the formation of ROS can be enhanced by simultaneously increasing the amount of OH^- and decreasing the portion of H^+ [41]. Therefore, pH equal to 9 was selected as the optimal pH.

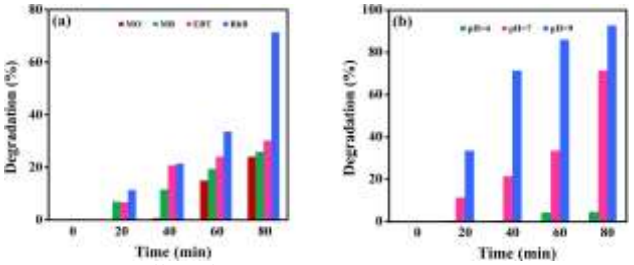

Fig. 9. (a) The effect of dye type on dye photodegradation, and (b) the effect of pH on RhB degradation in the presence of CQDs under UVA-light irradiation.

Kinetic of photocatalytic degradation

We investigated the photocatalytic degradation of dye throughout the optimal reaction conditions (RhB, and pH: 9) under UVA-light irradiation at 80 min and represented the obtained results in Fig. 10a. According to the evaluated kinetics of photocatalytic degradation reaction of RhB dye under UVA-light irradiation, the changes of dye concentration over time followed the design of pseudo-first-order (Eq. 3).[42]

$$-Ln\frac{C_t}{C_0} = kt \quad (3)$$

in which C_0 and C_t stand for the dye initial concentration and dye concentration at time t, respectively, while K refers to the reaction kinetics constant. In conformity to Fig. 10b, the kinetic constant of RhB degradation was reported to be -0.034 min^{-1} and the linear correlation coefficient was observed to be greater than 0.99.

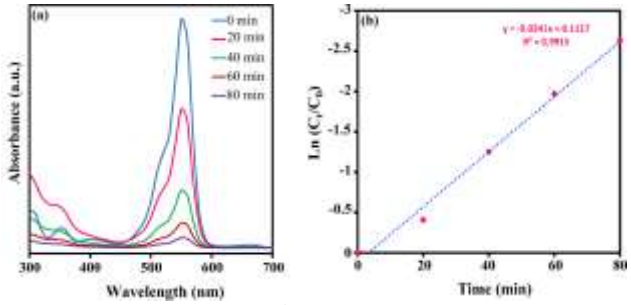

Fig. 10. (a) Decolorization of RhB dye using CQDs under UV-irradiation, and (b) the kinetic plots of pseudo-first-order model of RhB degradation by the exertion of CQDs.

Photocatalytic mechanism

Considering the functionalities of CQD as an absorber and catalyst, RhB dye is adsorbed on its surface while attracting external UVA-light irradiation as well. Therefore, the electrons (e^-) of CQDs are excited from the valence towards the conduction band that leads to the creation of holes (h^+) throughout the valence band. Thereafter, the excited electrons absorbed the molecular oxygen (O_2) and produce anion radical superoxide ($O_2^{\bullet-}$) or hydrogen peroxide (H_2O_2). The fabricated h^+ reacts with OH^- or H_2O molecules to form $OH^\bullet$ radicals,[28] which function as active species throughout the photocatalytic reaction and contribute to the degradation of EBT dye as the following (Eq. 4 to 9).

$$CQDs + h\nu \rightarrow CQDs^{*}\,(h^+ + e^-) \quad (4)$$

$$O_2 + e^- \rightarrow O_2^{\bullet-} \quad (5)$$

$$2H^+ + O_2 + 2e^- \rightarrow H_2O_2 \quad (6)$$

$$H_2O + h^+ \rightarrow OH^* + H^+ \quad (7)$$

$$H_2O_2 + O_2^{\bullet-} \rightarrow OH^* + O_2 + OH^- \quad (8)$$

$$RB + CQDs^{*}(h^+, e^-) \rightarrow \text{degradation} \quad (9)$$

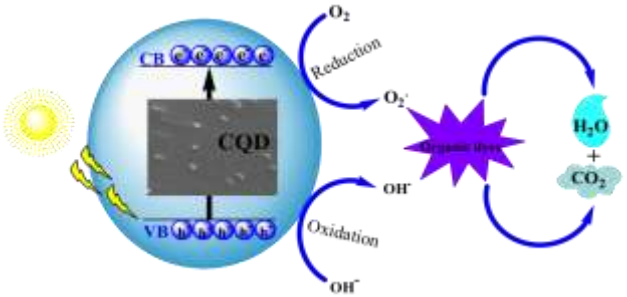

Fig. 11. Degradation mechanism of the dyes by the CQDs under UVA-light irradiation.

Cytotoxicity evaluation of the CQDs

The cytotoxicity of CQDs was assessed on the cancer CT26 cell line by the application of MTT assay. We exerted different concentrations of this product (16-1000 µg/mL) to evaluate the inhibitory concentration of cell growth. Fig. 12 displays the dependency of cell inhibition on the applied concentration while demonstrating the capability of CQDs in inhibiting cancer cells with an IC_{50} value of about 876 µg/mL.[43] Therefore, these CQDs can be suggested as an applicable candidate for the treatment of cancer.

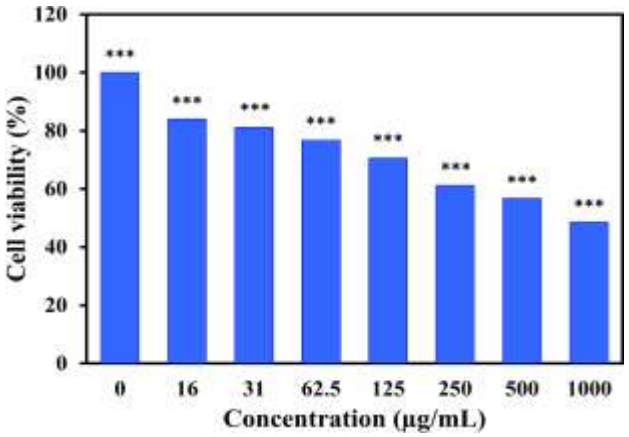

Fig. 12. Cytotoxicity effect of CQDs on CT26 cancer cell line by MTT assay.

4. CONCLUSION

The successful synthesis of CQDs was performed through a simple hydrothermal method by the exertion of TFL seeds as the carbon source. The prepared product contained a quasi-spherical morphology with an average size of about 7 nm. We also examined the cytotoxicity of synthesized CQDs on the CT26 cancer cell line by the means of the MTT method and observed concentration-dependent toxicity. This product was able to exhibit a high photocatalytic activity throughout the degradation of RhB dye under UVA-light irradiation and obtained a degradation percentage of 92% in 80 min. The degradation kinetics of RhB dye in the presence of CQDs was comparable to a pseudo-first-order model, while the degradation constant was reported to be 0.034 min^{-1}.

CONFLICTS OF INTEREST

The authors have declared no conflict of interest.

ACKNOWLEDGMENTS

The authors acknowledge their appreciation for all the technical support provided by Islamic Azad University of Tehran and Mashhad University of Medical Sciences.

AUTHOR INFORMATION

Corresponding Author

Majid Darroudi: Email: darroudim@mums.ac.ir, *ORCID*: 0000-0002-2624-7242.

Author(s)

Marzieh Rezaei, Azadeh Hekmat, Jamshidkhan Chamani, Kayvan Sadri

REFERENCES

1. S. Y. Lim, W. Shen, Z. Gao, *Chem. Soc. Rev.*, **2015**, *44*, 362-381.
2. L. Cao, X. Wang, M. J. Meziani, F. Lu, H. Wang, P. G. Luo, Y. Lin, B. A. Harruff, L. M. Veca, D. Murray, *J. Am. Chem. Soc.*, **2007**, *129*, 11318-11319.
3. Z. Liu, S. Tabakman, K. Welsher, H. Dai, *Nano Res.*, **2009**, *2*, 85-120.
4. Y. Wang, A. Hu, *J. Mater. Chem. C*, **2014**, *2*, 6921-6939.
5. X. Xu, R. Ray, Y. Gu, H. J. Ploehn, L. Gearheart, K. Raker, W. A. Scrivens, *J. Am. Chem. Soc.*, **2004**, *126*, 12736-12737.
6. Y. -P. Sun, B. Zhou, Y. Lin, W. Wang, K. S. Fernando, P. Pathak, M. J. Meziani, B. A. Harruff, X. Wang, H. Wang, *J. Am. Chem. Soc.*, **2006**, *128*, 7756-7757.
7. M. Nasrollahzadeh, M. Sajjadi, S. Iravani, R. S. Varma, Chemosphere, **2020**, 128005.
8. H. Yu, R. Shi, Y. Zhao, G. I. Waterhouse, L. Z. Wu, C. H. Tung, T. Zhang, *Adv. Mater.*, **2016**, *28*, 9454-9477.
9. H. Huang, S. Yang, Q. Li, Y. Yang, G. Wang, X. You, B. Mao, H. Wang, Y. Ma, P. He, *Langmuir*, **2018**, *34*, 250-258.
10. Y. Sun, X. Wang, C. Wang, D. Tong, Q. Wu, K. Jiang, Y. Jiang, C. Wang, M. Yang, *Mikrochim. Acta*, **2018**, *185*, 1-8.
11. T. Liu, C. Peng, Y. Ma, J. Ouyang, *Acta Chim. Sin.*, **2013**, *71*, 962-966.
12. P. Wang, J. -H. Liu, H. Gao, Y. Hu, X. Hou, G. E. LeCroy, C. E. Bunker, Y. Liu, Y. -P. Sun, *J. Mater.. Chem., C*, **2017**, *5*, 6328-6335.
13. Y. Liu, S. Han, *Food Anal. Methods*, **2017**, *10*, 3398-3406.
14. J. Li, J. Song, X. Liang, Q. Ma, L. Shen, Y. Guo, F. Feng, *Anal. Methods*, **2017**, *9*, 6379-6385.
15. S. Mitra, S. Chandra, S. H. Pathan, N. Sikdar, P. Pramanik, A. Goswami, *RSC Adv.*, **2013**, *3*, 3189-3193.
16. Z. Zeng, S. Chen, T. T. Y. Tan, F. -X. Xiao, *Catal. Today*, **2018**, *315*, 171-183.
17. R. Zhang, Z. Ding, *J. Anal. Test*, **2018**, *2*, 45-60.
18. L. Hu, Y. Sun, S. Li, X. Wang, K. Hu, L. Wang, X.-J. Liang, Y. Wu, *Carbon*, **2014**, *67*, 508-513.
19. M. Sabet, K. Mahdavi, *Appl. Surf. Sci.*, **2019**, *463*, 283-291.
20. Y. Liu, X. Li, Q. Zhang, W. Li, Y. Xie, H. Liu, L. Shang, Z. Liu, Z. Chen, L. Gu, *Angew. Chem. Int. Ed.*, **2020**, *59*, 1718-1726.
21. W. -J. Niu, Y. Li, R. -H. Zhu, D. Shan, Y. -R. Fan, X. -J. Zhang, *Sens. Actuators B: Chem.* **2015**, *218*, 229-236.
22. C. Fowley, N. Nomikou, A. P. McHale, B. McCaughan, J. F. Callan, *Chem. Commun.*, **2013**, *49*, 8934-8936.
23. Z. Yang, Z. Li, M. Xu, Y. Ma, J. Zhang, Y. Su, F. Gao, H. Wei, L. Zhang, *Nano-Micro. Lett.*, **2013**, *5*, 247-259.
24. M. A. Kanjwal, K. K. S. Lo, W. W. -F. Leung, *Sep. Purif. Technol.*, **2019**, *215*, 602-611.
25. I. Haq, A. Raj, *Bioremediation of Industrial Waste for Environmental Safety*, Springer, **2020**, 333-356.
26. X. Wei, R. Zhang, W. Zhang, Y. Yuan, B. Lai, *RSC Adv.*, **2019**, *9*, 39355-39366.
27. Y. Hu, R. Guan, C. Zhang, K. Zhang, W. Liu, X. Shao, Q. Xue, Q. Yue, *Appl. Surf. Sci.*, **2020**, *531*, 147344.
28. V. Ramar, S. Moothattu, K. Balasubramanian, *Sol. Energy*, **2018**, *169*, 120-127.
29. L. Zhou, Y. Lin, Z. Huang, J. Ren, X. Qu, *Chem. Commun.*, **2012**, *48*, 1147-1149.
30. A. Tyagi, K. M. Tripathi, N. Singh, S. Choudhary, R. K. Gupta, *RSC Adv.*, **2016**, *6*, 72423-72432.

31. M. J. Bojdys, J. -O. Müller, M. Antonietti, A. Thomas, *Chem. Eur. J.*, **2008**, *14*, 8177-8182.
32. H. Li, Z. Kang, Y. Liu, S. -T. Lee, *J. Mater. Chem.*, **2012**, *22*, 24230-24253.
33. J. Zheng, Y. Xie, Y. Wei, Y. Yang, X. Liu, Y. Chen, B. Xu, *Nanomaterials*, **2020**, *10*, 82.
34. J. Ke, X. Li, Q. Zhao, B. Liu, S. Liu, S. Wang, *J. Colloid Interface Sci.*, **2017**, *496*, 425-433.
35. K. Yao, X. Lv, G. Zheng, Z. Chen, Y. Jiang, X. Zhu, Z. Wang, Z. Cai, *Environ. Sci. Technol.*, **2018**, *52*, 14445-14451.
36. D. Hanaor, M. Michelazzi, C. Leonelli, C. C. Sorrell, *J. Eur. Ceram. Soc*., **2012**, *32*, 235-244.
37. A. Aghamali, M. Khosravi, H. Hamishehkar, N. Modirshahla, M. A. Behnajady, *J. Lumin.*, **2018**, *201*, 265-274.
38. T. Chatzimitakos, A. Kasouni, L. Sygellou, A. Avgeropoulos, A. Troganis, C. Stalikas, *Talanta*, **2017**, *175*, 305-312.
39. S. Sharma, V. Dutta, P. Singh, P. Raizada, A. Rahmani-Sani, A. Hosseini-Bandegharaei, V. K. Thakur, *J. Clean. Prod*., **2019**, *228*, 755-769.
40. A. Prasannan, T. Imae, *Ind. Eng. Chem. Res.*, **2013**, *52*, 15673-15678.
41. S. Malato, P. Fernández-Ibáñez, M. I. Maldonado, J. Blanco, W. Gernjak, *Catal. Today*, **2009**, *147*, 1-59.
42. Y. Cheng, M. Bai, J. Su, C. Fang, H. Li, J. Chen, J. Jiao, *J. Mater. Sci. Technol.*, **2019**, *35*, 1515-1522.
43. E. Arkan, A. Barati, M. Rahmanpanah, L. Hosseinzadeh, S. Moradi, M. Hajialyani, *Adv. Pharm. Bull*., **2018**, *8*, 149.